This article has been accepted for publication in IEEE International Instrumentation and Measurement Technology Conference Proceedings. This is the author's version which has not been fully edited and content may change prior to final publication. Citation information: DOI 10.1109/I2MTC48687.2022.9806511

Pulsed-Active Microwave Thermography

Logan M. Wilcox
Microwave Sensing (μSense) Laboratory
Department of Electrical and Computer Engineering
Missouri University of Science and Technology
Rolla, Missouri, USA
lmwc65@mst.edu

Mathias Bonmarin
Institute of Computational Physics
Zurich University of Applied Sciences
Winterthur, Switzerland
bmat@zhaw.ch

Kristen M. Donnell
Microwave Sensing (μSense) Laboratory
Department of Electrical and Computer Engineering
Missouri University of Science and Technology
Rolla, Missouri, USA
kmdgfd@mst.ed

Abstract—Active microwave thermography (AMT) is a thermographic nondestructive testing and evaluation technique that utilizes an electromagnetic-based excitation with a subsequent infrared measurement of the surface thermal profile of the material or structure of interest. AMT has been successfully applied to several aerospace and civil infrastructure applications. This work seeks to expand the performance of AMT by incorporating a signal processing technique common to traditional (flash-lamp) thermography, referred to as pulsed thermography (PT). PT operates on the premise of a pulsed excitation, as opposed to a constant or step excitation (ST) over a given time-period that is typical to traditional active thermography. This work applies the pulsed approach to AMT, herein referred to as P-AMT, and compares the thermal contrast (*TC*) and signal-to-noise ratio (*SNR*) of traditional and pulsed AMT inspections as applied to a moisture ingress detection need. The results suggest that the optimal heating time (indicated through *SNR*) for P-AMT is less than that of traditional AMT with a reduced overall (absolute) temperature. This is important as it relates to any inspection with concerns for thermal damage as well an overall reduction in required inspection time.

Keywords—Nondestructive Testing and Evaluation (NDT&E), Pulsed Thermography (PT), Active Microwave Thermography (AMT), Thermal Contrast (TC), Signal-to-Noise Ratio (SNR)

I. Introduction

The area of nondestructive testing and evaluation (NDT&E) encompasses a multitude of techniques to detect and quantify damage, defects, or flaws in a specimen under test (SUT). The technique selected for a given inspection need depends on several factors including the geometry of the structure under consideration, materials involved, defect type of interest, and so forth. Thermography is one such technique has been successfully applied to many industries including civil infrastructure and aerospace, amongst others. Thermographic inspection results are easy to interpret, and the technique itself is popular due to its non-contact inspection capability and potential for large-scale inspections [1]. In general, thermography utilizes both passive and active thermal excitations. Passive thermography generally refers to a solar excitation, whereas active thermography incorporates a specific type of thermal excitation source that is applied over a specified duration of time [1]. Following the application of thermal energy, the surface thermal profile of the SUT in question is viewed using an infrared (IR) or thermal camera. These active sources include flash lamp [2], laser [3], induction [4], ultrasound transducers [5], and more recently, a microwave-based excitation [6]-[9].

Regardless of the excitation method, thermographic inspections can take advantage of the well-established signal processing techniques common to this inspection approach. One such technique that is of interest to this work is pulsed thermography (PT) [1], [10]. PT requires an active thermographic inspection and utilizes short (modulated) bursts of energy directed towards the SUT. PT has been applied to active thermographic inspection methods such as heat lamp [2], induction [4], and, as is the topic of this work, microwave-based inspections. In the case of a microwave-based excitation, the thermal excitation is (primarily) generated through electromagnetic energy that is absorbed into dielectric materials. This approach will herein be referred to as active microwave thermography (AMT) [6]-[9]. AMT is a relatively new NDT&E technique that has been successfully applied for inspection of a variety of infrastructure and aerospace-related needs [6]-[9]. Utilizing a microwave-based excitation offers a unique way to accomplish a thermographic inspection in that the thermal excitation can be tailored to the inspection need via electromagnetic parameters such as frequency and polarization. This research expands the concept of AMT by applying PT, with the updated approach herein referred to as Pulsed-Active Microwave Thermography, or P-AMT.

II. Background

As mentioned, AMT utilizes an infrared camera to observe changes in the surface temperature of a SUT during an inspection. While thermal measurement via the camera does provide a quantitative representation (absolute temperature) of the thermal changes on the surface, an approach that incorporates the temperature increase (with respect to ambient) during inspection, as opposed to the overall absolute temperature, is preferred [7]. To this end, to quantitatively assess an AMT thermal image, the thermal contrast (*TC*) is considered and is defined as the difference in temperature increase between defective and sound (defect-free) locations, as defined in (1):

$$TC(t) = [T_D(t) - T_{aD}] - [T_S(t) - T_{aS}] \quad (1)$$

This article has been accepted for publication in IEEE International Instrumentation and Measurement Technology Conference Proceedings. This is the author's version which has not been fully edited and content may change prior to final publication. Citation information: DOI 10.1109/I2MTC48687.2022.9806511

where $T_D(t)$ and $T_S(t)$ are temperatures of the defect and sound locations after thermal excitation, respectively, and T_{aD} and T_{aS} are the ambient temperatures of the defect and sound locations, prior to any excitation, respectively.

Signal-to-noise ratio (*SNR*) is another parameter that can be utilized to quantitatively analyze an AMT inspection result. SNR considers the variation of surface temperature in the defect and sound areas, as defined in (2) [11]:

$$SNR(t) = 20log_{10}\frac{|\mu_D(t)-\mu_S(t)|}{\sigma_S(t)} \quad (2)$$

where $\mu_D(t)$ is the mean surface temperature of the defect location, and $\mu_S(t)$ and $\sigma_S(t)$ are the mean and standard deviation, respectively, of the surface temperature of a sound area. These quantities are calculated as a function of time, *t*, as:

$$\mu(t) = \frac{1}{N_p}\sum_{p=1}^{N_p}\Delta T_p(t) \quad (3)$$

$$\sigma(t) = \sqrt{\frac{1}{N_p}\sum_{p=1}^{N_p}\left[\Delta T_p(t)-\mu(t)\right]} \quad (4)$$

where $\Delta T_p(t)$ is the temperature at pixel (within the thermal image), *p,* with respect to time, *t,* and N_p refers to the total number of pixels in specified defective, or sound, area.

III. Electromagnetic-Thermal Simulations

To illustrate the potential application of pulsed techniques to AMT inspections, a coupled electromagnetic-thermal simulation was performed using CST MultiPhysics Studio™. These simulations considered a rubber structure undergoing water ingress (i.e., the SUT), as illustrated in Fig. 1. The rubber sample has a cross-section of 100×100 mm², and a thickness of 13 mm. The water ingress is represented by a volume of 0.05 mL that is placed 4 mm deep from the inspection surface of the SUT.

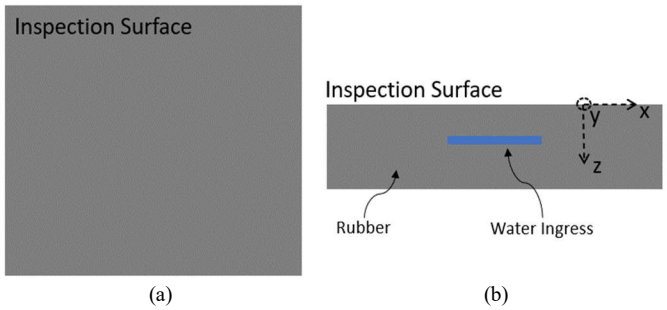

Fig. 1. Top (a) and side (b) illustrative views of the SUT.

As mentioned above, the thermal excitation in AMT is usually achieved through dielectric absorption. Generally speaking, the ability of a dielectric material to absorb microwave energy is quantified though the imaginary portion of the complex dielectric properties, ε. When referenced to free-space, these properties are denoted as $\varepsilon_r = \varepsilon_r' - j\varepsilon_r''$. The imaginary part ($\varepsilon_r''$) or loss factor, describes how well a material absorbs microwave energy (and is of interest here). The real part (ε_r'), or permittivity, quantifies energy storage. As it relates to the simulations presented here, the moisture ingress (defect of interest) has a very high loss factor and therefore, when undergoing an AMT inspection, acts as a volumetric heat source due to its strong ability to absorb microwave energy. The surrounding rubber structure is assumed to be a low loss material, and hence will not undergo a thermal increase in the same way as the moisture. The heat generated through this thermal source diffuses through the rubber structure and becomes observable on the surface. The electromagnetic and thermal properties utilized in the simulation are shown in Table 1. A 2.4 GHz signal (selected due to the high absorption of microwave energy by water at this frequency [6], [12]) with a total power of 50 W is assumed to be incident on the top side of the structure (see Fig. 1a) for 90 seconds (i.e., a heating time of 90 sec). The energy is assumed to radiate from a standard gain horn antenna placed 13 cm from the surface of the SUT.

Table 1: Relevant properties of water and rubber [12], [13], [14]

Material	*Property*	*Value*
Water	Relative Permittivity, ε_r'	77
	Relative Loss Factor, ε_r''	9
Rubber	Relative Permittivity, ε_r'	2.4
	Relative Loss Factor, ε_r''	0
	Thermal Diffusivity, α	0.11 mm²/s
	Thermal Conductivity, k	0.16 W/m² ·K

This coupled simulation considers both electromagnetic and thermal behaviors, capturing the incident electric field that is absorbed by the water ingress (since the rubber structure is assumed to be lossless). Then, this absorbed energy is translated to generated heat, Q, which subsequently diffuses through the rubber and is calculated as:

$$Q = 2\pi f \varepsilon_r' \varepsilon_r'' |E|^2 \quad (5)$$

where f is the frequency and E is the incident electric field (i.e., related to the radiated microwave power of 50 W). The subsequent thermal diffusion through the rubber is related to the thermal conductivity, K_T, the specific heat, C_T, and density, ρ, of the rubber (see Table 1). The thermal boundary conditions of the simulation were selected in order to model an infinite expansion of the material in the lateral direction (perpendicular to the direction of the incident energy, or the x- and y-directions in Fig. 1b), leaving heat diffusion as the only method of heat transfer in these directions. The thermal simulation boundary condition on the inspection surface and back side of the SUT is

This article has been accepted for publication in IEEE International Instrumentation and Measurement Technology Conference Proceedings. This is the author's version which has not been fully edited and content may change prior to final publication. Citation information: DOI 10.1109/I2MTC48687.2022.9806511

considered adiabatic (i.e., heat transfer is absent through the boundary).

Using this model, simulations of traditional AMT and P-AMT were conducted to facilitate a performance comparison between the two approaches. As traditional AMT utilizes a constant illumination of the SUT for a specified heating time, for this work, a period of 90 seconds was chosen to ensure a substantial thermal increase was generated. In contrast to the constant illumination of AMT, P-AMT utilizes a square-wave modulation on the amplitude of the incident microwave signal. For this simulation, the modulation rate has a period of 2 seconds. Fig. 2 shows the surface thermal profiles for AMT and P-AMT, respectively.

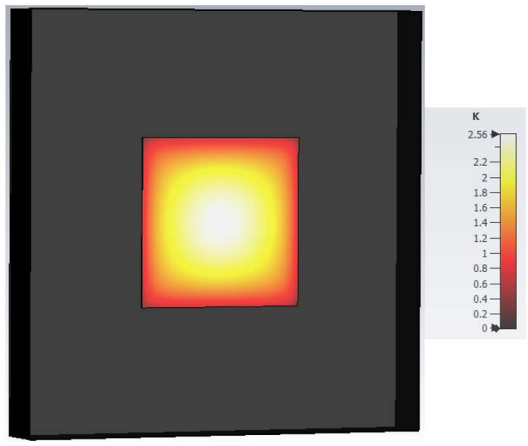

(a)

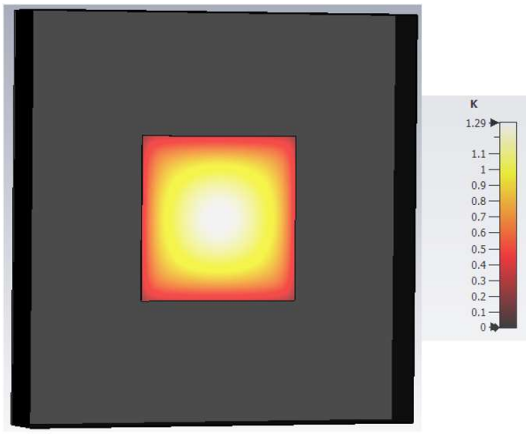

(b)

Fig. 2. (a) AMT and (b) P-AMT surface thermal profiles from the electromagnetic-thermal simulation.

Fig. 3 displays the simulated *TC* (a) and *SNR* (b) of traditional AMT and P-AMT with a total of 90 seconds of microwave energy absorption time. This means that the illuminating/heating time for AMT was 90 sec, but the heating time for P-AMT was 180 sec (to compensate for the fact that the illuminating signal is modulated "on" and "off" every 2 seconds, resulting in a 50% duty cycle). In other words, to ensure that the sample underwent 90 sec of signal illumination, 180 sec of pulsed signal was necessary. As seen in Fig. 3a, traditional AMT provides a higher *TC* than P-AMT due to the continuous heating process. However, both results are detectable (assuming a thermal sensitivity of 30 m°K for a typical thermal camera, such as the one used later for measurements). In addition, the rate of thermal increase is also greater during the respective heating time of AMT as compared to that of P-AMT. Both points support the P-AMT inspection approach as the lower-risk approach as it relates to potential thermal damage. It can also be seen that the rates of cooling for AMT and P-AMT are similar, with ambient conditions reached (i.e., $TC = 0$) in a similar fashion.

The *SNR* for traditional AMT and P-AMT is shown in Fig. 3b. *SNR* is particularly useful as it can indicate when an optimal heating time has been achieved (i.e., when the *SNR* no longer increases with heating time) [11]. As it relates to this work, the *SNR* for AMT has a larger maximum value than that of P-AMT for the heat duration considered, but as asymptotic behavior is not evident yet, it cannot be assumed that this heating time (90 sec) is ideal. However, asymptotic behavior is more evident for the *SNR* of P-AMT, indicating that optimal heating time may be reduced for this inspection when P-AMT is applied (here, on the order of 100 sec). This has important ramifications not only as it relates to maximum thermal considerations (mentioned above), but also to overall required inspection times.

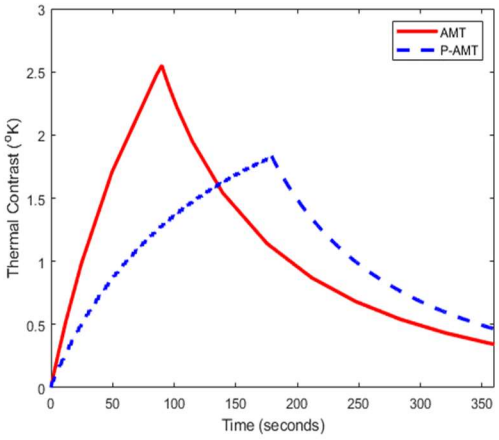

(a)

This article has been accepted for publication in IEEE International Instrumentation and Measurement Technology Conference Proceedings. This is the author's version which has not been fully edited and content may change prior to final publication. Citation information: DOI 10.1109/I2MTC48687.2022.9806511

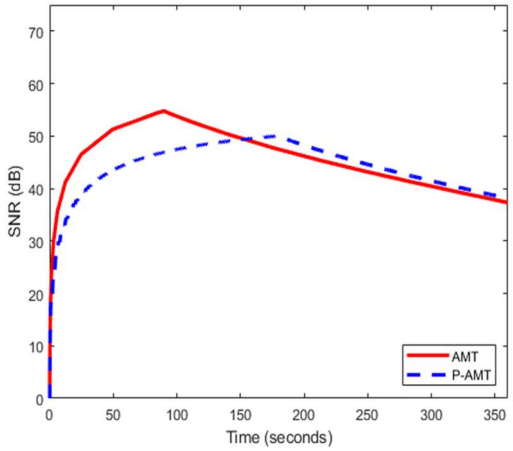

(b)

Fig. 3. (a) *TC* and (b) *SNR* of traditional AMT and P-AMT with 90 seconds of total microwave absorption time.

To further compare traditional AMT with P-AMT, a simulation was conducted when the excitation period was limited to 90 seconds for both approaches. In this case, the total absorption time for AMT is twice that of P-AMT, due to the modulated nature of P-AMT. The results for *TC* and *SNR* are shown in Fig. 4. As seen in Fig. 4a, the maximum *TC* for traditional AMT is approximately double than that P-AMT. This is as expected, due to the nature of the square wave modulation applied here (i.e., 50% duty cycle). Moreover, for this inspection, the *SNR* for each is very similar, further supporting the point that utilizing P-AMT can effectively reduce inspection-induced thermal stresses since the absolute temperature is less while maintaining the same level of confidence in the overall inspection results (i.e., *SNR*).

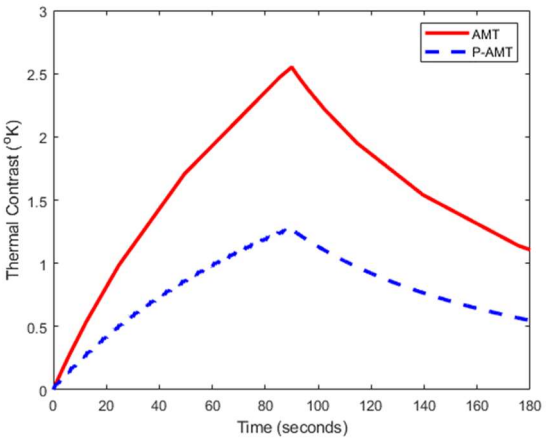

(a)

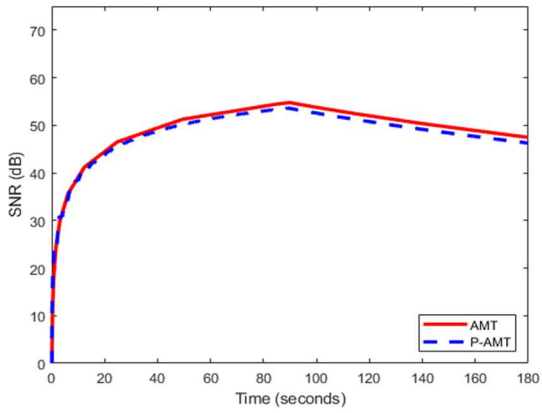

(b)

Fig. 4. (a) *TC* and (b) *SNR* of traditional AMT and P-AMT with 90 seconds of microwave illumination.

IV. Measurements

Measurements were conducted to support and confirm the simulated results above. To this end, the AMT system (with modified signal control added to implement P-AMT) used for these measurements is schematically illustrated in Fig. 5.

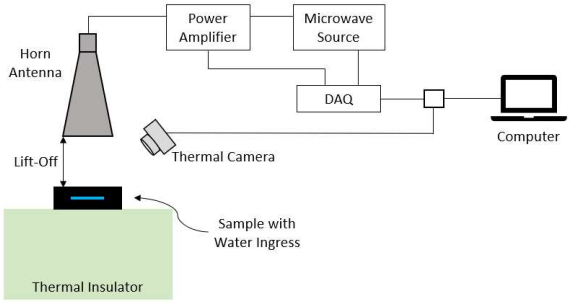

Fig. 5. Schematic of the measurement system.

The system includes a 50 W amplifier and utilizes a horn antenna with a length of 40 cm, aperture dimensions of 23×17 cm², and operates at a frequency of 2.4 GHz. A FLIR T430sc infrared camera with a thermal sensitivity of 30 m°K was used to capture the surface thermal profile of the SUT. A data acquisition unit (DAQ) and computer are used to control and synchronize the microwave source, power amplifier, and thermal camera. For P-AMT, the modulation signal is also managed and applied to the amplifier through the DAQ. The distance between the horn antenna and the SUT, known as the lift-off distance, was 13 cm. The SUT consists of 1 mL of water, added to a 2 × 2 cm² piece of paper towel, that was placed between two pieces of rubber. The bottom piece is 1.5 cm thick, and the top piece is 4 mm (see Fig. 1b). The SUT was centered with respect to the horn antenna aperture and placed on top of a thermal insulator (polystyrene foam) to avoid thermal energy loss on the back side of the SUT (i.e., an adiabatic condition). The results of the inspection are shown in Fig. 6 (*TC*) and Fig. 7 (*SNR*) for a heating time of 90 sec for traditional AMT and P-AMT.

This article has been accepted for publication in IEEE International Instrumentation and Measurement Technology Conference Proceedings. This is the author's version which has not been fully edited and content may change prior to final publication. Citation information: DOI 10.1109/I2MTC48687.2022.9806511

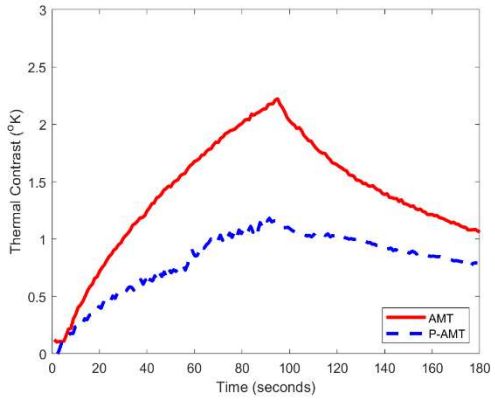

Fig. 6. *TC* of AMT and P-AMT measurements.

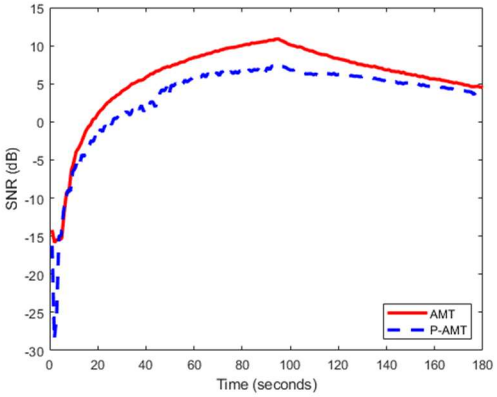

Fig. 7. *SNR* of AMT and P-AMT measurements.

As can be seen in Fig. 6, for traditional AMT, the *TC* is 1.05 °K at the end of the inspection and achieves a max *TC* of 2.22 °K at 90 sec. For P-AMT, the *TC* is 0.80 °K at the end of the inspection and achieves a max *TC* of 1.25 °K at 90 sec. These results are relatively close, within a tenth of a °K, to those of the coupled electromagnetic-thermal simulation. It is also evident that the response of the AMT inspection is approximately double that of the P-AMT. This is to be expected given the 50% duty cycle (with the difference attributed losses not accounted for in the model). Additionally, as seen in Fig. 7, the *SNR* for P-AMT reaches asymptotic behavior after ~90 sec, similar to the ~100 sec mark of the simulated results. Conversely, it is not reached during the traditional AMT inspection. These results further support the application of PT to AMT, offering a reduction in absolute thermal increase of the sample and reduced inspection times, both important practical aspects.

A last point of note is related to measurement uncertainty. Uncertainties in the measurements may result from several parameters including variation in the amount of water ingress, ambient temperature during measurements, etc. Within these potential contributors, the experimental process was controlled in such a way as to negate concerns resulting from the SUT (e.g., volume of water ingress, etc.). However, the effect of ambient temperature is considered in Eq. (1) through the calculation of *TC*. In addition, as shown in Eq. (2)-(4), the calculation of *SNR* includes the standard deviation of the surface temperature of a sound area of the SUT. In this way, measurement uncertainly due to ambient temperature fluctuations is accounted for within the process.

The effect of duty cycle was also investigated experimentally. More specifically, additional duty cycles of 25% and 75% (keeping with the square wave modulation) were used for measurements with the same experimental setup as above and illustrated in Fig. 5. The 25% duty cycle incorporates an "on" period of 1 sec, while the "off" period is increased to 3 sec, for a total heating time of 90 sec. The inverse was done for the 75% duty cycle (i.e., 3 sec "on" and 1 sec "off" for a heating time of 90 sec). The results for these inspections are shown in Fig. 8 (*TC*) and Fig. 9 (*SNR*). Included in these figures are the results of 100% (traditional AMT) and 50% duty cycles (as shown in Figs. 6-7) for comparison.

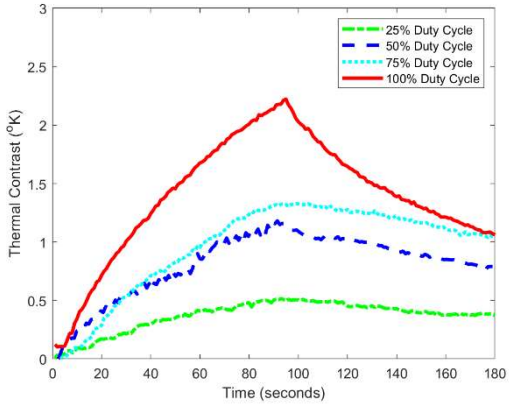

Fig. 8. *TC* of P-AMT measurements taken with 25%, 50%, 75%, and 100% (i.e., traditional AMT) duty cycles.

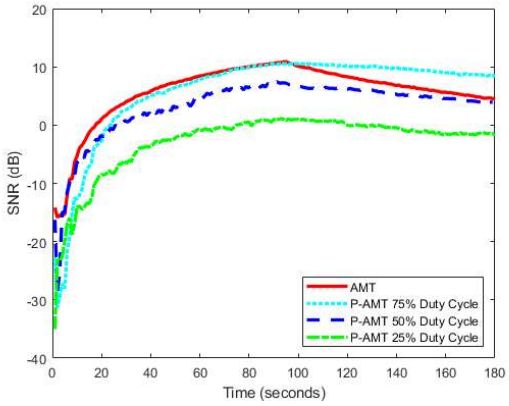

Fig. 9. *SNR* of P-AMT measurements taken with 25%, 50%, 75%, and 100% (i.e., traditional AMT) duty cycles.

As can be seen in Fig. 8, the TC increases as expected with increasing duty cycle. It is interesting to note that the maximum *TC* achieved by traditional AMT (100% duty cycle) after the heating period of 90 sec is 0.89 °K greater than the maximum *TC* achieved with a 75% duty cycle. It can also be seen that the maximum *TC* for the other three duty cycles span from 0.52 °K to 1.33 °K, a smaller range that what was detected from 75% to 100%. Moreover, with a thermal sensitivity of 0.030 °K, the effect of the defect in this inspection was detectable with all duty

cycles considered. This indicates that the required energy can be substantially reduced when a modulated approach is taken. This is further illustrated by the results of Fig. 9, where the corresponding *SNR* for all four duty cycles is shown. As the established metric for detectability in thermographic inspections is an *SNR* = 0 [15], this metric was achieved at 75 sec, 28 sec, 24 sec, and 18 sec, for 25%, 50%, 75%, and 100% duty cycle, respectively. As such, these results further support the conclusion that inspection time and overall temperature increase can be optimized for AMT inspections with the inclusion of pulsed techniques.

V. Conclusion

The potential for PT to be utilized with a microwave-based excitation source was investigated. This was achieved by a coupled, electromagnetic-thermal simulation that considered traditional and pulsed AMT. Representative measurements were also completed. Both simulated and measured results indicate that a P-AMT-based inspection facilitate an overall reduction in *TC* (i.e., a reduced absolute thermal increase). The *SNR*, a metric that can be used to determine optimal heating times, indicated that P-AMT inspections require overall less heating time than a traditional AMT inspection. Further investigation of this approach will include the application of PT to different types of defects and inspection needs, along with consideration of other modulation waveforms (and the effect of additional duty cycles) for the pulsed modification.

References

[1] X. P. Maldague, “Theory and Practice of Infrared Technology for Nondestructive Testing”. New York, NY, USA: Wiley, 2001.

[2] P. Broberg "Surface crack detection in welds using thermography" NDT E Int. vol. 57 pp. 69-73 Jul. 2013.

[3] Y. An J. M. Kim and H. Sohn "Laser lock-in thermography for detection of surface-breaking fatigue cracks on uncoated steel structures" NDT E Int. vol. 65 pp. 54-63 Jul. 2014.

[4] M. Noethen K.-J. Wolter and N. Meyendorf "Surface crack detection in ferritic and austenitic steel components using inductive heated thermography" Proc. 33rd IEEE Int. Spring Seminar Electron. Technol. (ISSE) pp. 249-254 May 2010.

[5] Mendioroz, A., R. Celorrio, and A. Salazar. "Ultrasound excited thermography: an efficient tool for the characterization of vertical cracks." Measurement Science and Technology, vol. 28, no. 11, Oct. 2017.

[6] A Mirala, A. Foudazi, M. T. Ghasr, and K. M. Donnell, “Active Microwave Thermography to Detect and Locate Water Ingress,” IEEE Trans. Instrum. Meas., vol. 69, no. 12, pp. 9774-9783, Dec. 2020.

[7] A. Foudazi, C. A. Edwards, M. T. Ghasr, and K. M. Donnell, “Active Microwave Thermography for Defect Detection of CFRP-Strengthened Cement-Based Materials,” IEEE Trans. Instrum. Meas., vol. 65, no. 11, pp. 2612-2620, Nov. 2016.

[8] A. Mirala, M. T. A. Qaseer and K. M. Donnell, "Health Monitoring of RAM-Coated Structures by Active Microwave Thermography," in IEEE Transactions on Instrumentation and Measurement, vol. 70, pp. 1-11, 2021.

[9] A. Mirala and K. M. Donnell. “Active Microwave Thermographic Measurement of In-Plane Thermal Diffusivity,” in Proc. IEEE Int. Instrum. Meas. Technol. Conf. (I2MTC), May 2020, pp. 1-5.

[10] L. Junyan, W. Yang, and D. Jingmin, “Research on thermal wave processing of lock-in thermography based on analyzing image sequences for NDT,” Infrared Physics and Technology, vol. 53, no. 5., pp. 348-357, June 2010.

[11] C. Ibarra-Castanedo, J. Piau, S. Guilbert, N. P. Avdelidis, M. Genest, A. Bendada, and X. Maldague, “Comparative study of active thermography techniques for the nondestructive evaluation of honeycomb structures,” Research in Nondestructive Evaluation, vol. 20, no. 1, pp. 1-31, 2009.

[12] U. Kaatze, “Complex permittivity of water as a function of frequency and temperature,” J. Chem. Eng. Data, vol. 34, no. 4, pp. 371–374, Oct. 1989.

[13] W. M. Haynes, Ed., CRC Handbook of Chemistry and Physics. Boca Raton, FL, USA: CRC Press, 2016.

[14] E. M. Ortt et al, “A Device for Evaluating the Multiaxial Finite Strain Thermomechanical Behavior of Elastomers and Soft Tissues,” Journal of Applied Mechanics, vol. 67, pp. 465-471, Sep. 2000.

[15] K. Srinivas, A. O. Siddiqui, and J. Lahiri, “Thermographic inspection of composite materials,” In Proc. National Seminar on Non-Destructive Evaluation, vol. 12, pp. 7-9, 2006.